UDC 539.17

[2]Burtebayev N., [1,2*]Mukhamejanov Y.S., [1,2]Alimov D.K.,
[2]Kerimkulov Zh.K., [3]Janseitov D.M., [4]Trzaska W.H.

[1]Physics and Technology Department, al-Faraby KazNU, Almaty, Kazakhstan,
[2]Institute of Nuclear Physics, Almaty, Kazakhstan,
[3]Physics and Technology Department, Eurasian National University, Astana, Kazakhstan
[4]University of Jyväskylä, Jyväskylä, Finland
*e-mail: y.mukhamejanov@gmail.com

# Comparative analysis of elastic and inelastic scattering of d and α-particles from $^{11}$B

**Abstract.** Experimental angular distributions of elastic and inelastic scattering of deuterons at $E_d$=14.5 MeV and alpha particles at $E_\alpha$=29, 40.5 and 50.5 MeV from nuclei $^{11}$B were measured on the extracted beam of isochronous cyclotron U-150M at the Institute of Nuclear Physics (Almaty, Kazakhstan) within angular range of 10-150 degrees in laboratory system. The analysis of experimental data on elastic scattering of deuterons and alpha particles from $^{11}$B nucleus was made within the optical model and double folding model with literature data at different energies of the incident particles. The analysis of experimental data on inelastic scattering of deuterons and alpha particles from $^{11}$B nucleus was made within the coupled channels method. The calculations were made using FRESCO computer code. The radii of the $1/2^-$ (2.125 MeV), $5/2^-$ (4.445 MeV), $7/2^-$ (6.742 MeV) and "exotic" $3/2^-$ (8.56 MeV) states of $^{11}$B were determined within the modified diffraction model. As a result of the analysis, the optimal parameters of the phenomenological optical potentials and double folding potentials were determined for $^{11}$B+d and $^{11}$B+α systems.

**Key words:** deuterons, α-particles, optical model, double folding, modified diffraction model, nuclear radii, fresco.

## Introduction

Study of elastic and inelastic scattering processes of light charged particles, such as deuterons and alpha particles, is one of the main sources of the information about the nuclear potentials, which are used to calculate the wave functions describing the relative motion of the colliding particles, as well as information about the properties of ground and low lying excited sates of nuclei. These processes take place during collisions of alpha particles at energies of tens of MeV and allow obtaining highly valuable information about the structural characteristics of nuclei, such as deformation parameters and nuclear radii. So called direct transitions from initial to some final state of the nucleus without any intermediate processes usually take place at mentioned energies. This is the reason why those kinds of transitions are the most convenient tool for receiving spectroscopic information about properties of various states of nuclei. This is due to the fact that direct mechanism as is dominates in direct processes and they do not mix much with more complex reactions and do not cause mixing of numerous excited states. For this reason elastic and inelastic processes quite selectively excite single-particle and quasi-hole as well as different types of collective states. That is why they are called the most pure method of studying mentioned states.

Of particular interest from the point of view of studying excited neutron halo-states of light nuclei are the states of $^{11}$B nucleus, where both "exotic" cluster configuration (2α+t), and the shell model structure can co-exist at the same time. Indeed, several studies have suggested that low-lying states of $^{11}$B, basically, have a shell structure, while the cluster structures are easily traced in the states with negative parity above or near the threshold of breakup into clusters.

## Experimental details

The experiment was carried out at U-150M cyclotron at the Institute of Nuclear Physics Institute of Nuclear Physics (INP) (Almaty, Kazakhstan) which allows to accelerate protons up to 30 MeV, deuterons up to 25 MeV, $^3$He up to to 60 MeV and

 

alpha-particles up to 50 MeV. Charged particles in cyclotron are formed in source, located in the central part of camera in an arc discharge when supplying corresponding gas (hydrogen, deuterium, helium-3, helium-4). They are accelerated in the interpolar space of 1.5-meter magnet when particles fly between the dees.

Transportation scheme of accelerated ions beam from a cyclotron chamber to the scattering chamber, located at 24 meters away from the beam is shown in Figure 1. It includes a quadruple lens system, two bending, separating, two targeting magnets and collimators system. All these setups with the targeting and correction elements provide a charged particles beam at the target with angle spread not more than 0,4° and 3 mm in diameter. Adjusting positions of the collimator and the center of scattering chamber with respect to the ion guide axis was carried out by optical method and controlled by means of a 12-quartz screens and television cameras that transmit image to the cyclotron remote control.

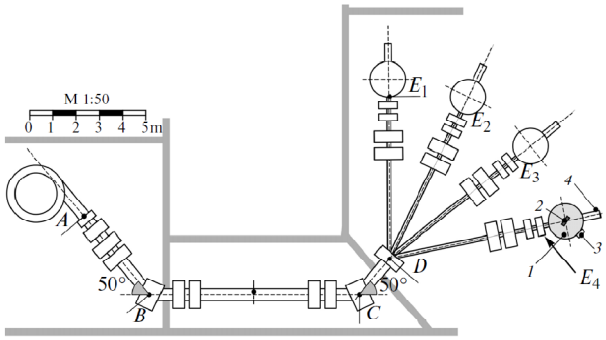


a

A, B, C, D, and E are the characteristic points and the accelerated ion beam bending points; (1) scattering chamber; (2) target; (3) rotating scattered particle detector; (4) Faraday cup.

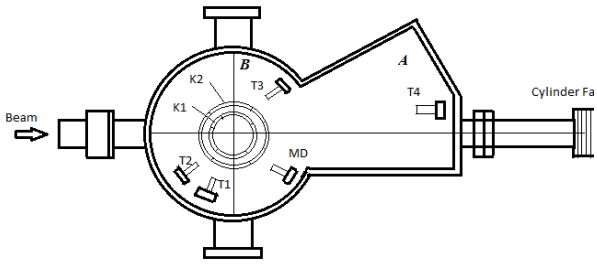


b

$K_1$ and $K_2$ – independently rotating rings with step engine drives; $T_1$-$T_4$ – telescopes of E-ΔE detectors attached to $K_1$ and $K_2$; MD – detector for monitoring scattered beam

**Figure 1** – (a) U-150M isochronous cyclotron with adjustable ion energy and the ion beam transport line to the scattering chamber. (b) Scattering chamber

Vacuum scattering chamber (60 cm in diameter) was used for measurements of angular distributions of nuclear reactions products with charged particles (Figure 2).

The chamber, made of stainless steel, consists of hollow cylinder B with internal diameter of 715 mm, 370 mm height and so called "pocket" A which is an additional volume extended along beam direction. There are three (E-ΔE) telescopes of silicon semiconductor detectors, which cover the scattering angles of 10–70° in the main volume B of the chamber. A fourth telescope with independent drive, designed for covering the measurements in the angular range of 2–20° is located in volume A. Considerable distance from the target (1000 mm) allows to reduce 10–15 times the load on detecting apparatus due to the elastic scattering measurements at extremely small angles. Monitoring window with a diameter of 290 mm located on the top cover of the chamber allows visual inspection of the experimental situation (angles of the telescopes, the state of the target, etc.).

For optimal focusing of the accelerated $^4He$ ions on the target, two collimators of diameter 2 mm were used. Pumping system which includes a high-vacuum turbo molecular pumps and pre-evacuation was tested and showed good results in achieving high vacuum inside the chamber of about $2.3 \times 10^{-6}$ Pa.

Targets were thin metal foils made of boron-11 isotope. $^{11}B$ isotopes were sputtered on a glass by electron sputtering method on VUP-5 setup. The foil was later taken off the glass on a surface of distilled water by dissolving intermediate salt layer.

Target thickness was determined at linear accelerator UKP-2-1 at INP. For determining the thickness of boron $^{27}Al(p,\gamma)^{28}Si$ reaction yield curves in the region of resonance at $E_p$=992 keV [1] were measured using aluminum foil and the sputtered target. The shift of this resonance in the

$^{27}$Al(p,γ)$^{28}$Si reaction due to protons energy loss while passing $^{11}$B film was 62.0 keV which responds to the target thickness equal to 320 μg/cm$^2$. This method allowed determining target thickness with accuracy not more than 5%.

The (*E-ΔE*) method was used in the registration and identification of reactions products. The method is based on simultaneous measurement of specific energy losses of charged particles in matter (*dE*/*dx*) and the total kinetic energy *E*. In the telescope of detectors "*E-ΔE*", *ΔE* - detector is a surface-barrier silicon detector- company ORTEC- thick active layer of 30 to 200 μm with thin inlet (~ 40μg/cm$^2$ Au) and outlet (~40μg/cm$^2$ Al) windows. The complete absorption *E* detector is used as a stop detector- company ORTEC high-purity silicon; thickness of 2 mm.

**Elastic scattering**

The analysis of elastic scattering of deuterons and alpha particles from $^{11}$B nuclei including literature data at $E_d$=11.8, 13.6 and 27.7 MeV [2-4] and $E_\alpha$=40.5, 50.5 [5], 48.7 [6] and 54.1 MeV [6] was made within both phenomenological optical model (OM) and semi-microscopic double folding (DF) model using computer code FRESCO [7]. Within phenomenological approach elastic scattering is described by complex radius dependent Woods-Saxon shaped interaction potential:

$$U(r) = -V\, f\,(x_V) - i\,[Wf(x_W)] + V_C(r), \quad (1)$$

where $f(x_i) = (1+\exp(x_i))^{-1}$, $x_i = (r - R_i)/a_i$, $R_i = r_i A^{1/3}$, $V_C(r)$ – Coulomb potential of uniformly charged sphere with radius $R=1.28A^{1/3}$ fm, *V* – depth of real part of the potential, *W* – depth of the imaginary part of the potential, *r* and *a* are the values of radius and diffuseness, respectively. Taking into account compact size of the incident particle, we while analyzing the data at high energies limited with volume type of absorption potential for the imaginary part. The results of the comparison of calculated values of differential cross sections with the experimental angular distributions are given in Figure 3.

It is common to use the folding model to calculate the real potential and to use a Woods-Saxon (WS) form for the imaginary potential. Given correct nuclear densities as inputs for the DF calculation, it remains necessary to have an appropriate in-medium NN interaction for a reliable prediction of the (real) nucleus–nucleus OP. Most of the 'microscopic' nuclear reaction calculations so far still use different kinds of the effective NN interaction. Very popular choices have been the so-called M3Y interactions which were designed to reproduce the *G*-matrix elements of the Reid [8] and Paris [9] free NN potentials in an oscillator basis (further referred to as M3Y-Reid and M3Y-Paris interaction, respectively). The original M3Y interaction is density independent and given in terms of the Yukawa functions as follows:

M3Y-Reid:

$$v_D(s) = 7999.0\frac{\exp(-4s)}{4s} - $$

$$-2134.25\frac{\exp(-2.5s)}{2.5s}, \quad (2)$$

$$v_{EX}(s) = 4631.38\frac{\exp(-4s)}{4s} -$$

$$1787.13\frac{\exp(-2.5s)}{2.5s} - 7.8474\frac{\exp(-0.7072s)}{0.7072s},$$

M3Y-Paris:

$$v_D(s) = 11061.625\frac{\exp(-4s)}{4s} -$$

$$-2537.5\frac{\exp(-2.5s)}{2.5s}, \quad (3)$$

$$v_{EX}(s) = -1524.25\frac{\exp(-4s)}{4s} -$$

$$-518.75\frac{\exp(-2.5s)}{2.5s} - 7.8474\frac{\exp(-0.7072s)}{0.7072s},$$

The Yukawa strengths in equations (2) and (3) are given in MeV, and *s* is the distance between the two interacting nucleons. These interactions, especially the M3Y-Reid version, have been used with some success in the DF model calculations for the interaction between heavy ions (HI) at low energies [10], with the elastic data usually limited to the forward scattering angles and, thus, sensitive to the OP only at the surface. The inclusion of an explicit density dependence was needed to account for a reduction in the strength of the nucleus–nucleus interaction that occurs at small *R* where the overlap density of the nuclear collision increases. An early version of the density dependence of the M3Y-Reid interaction was constructed by Kobos *et al* [10] based upon the *G*-matrix results obtained by Jeukenne *et al* [11]. It was dubbed as the DDM3Y interaction and has been used to improve the folding model description of the elastic *α*-nucleus [11-13]

and light HI [14] scattering. The obtained parameters of potentials are given in Table 1. The comparison of experimental differential cross sections of elastic scattering of deuterons and alpha particles with the calculations within OM and DF are given in figures 2 and 3.

**Table 1** – Parameters of optical and folding potentials for deuterons scattering from $^{11}$B nuclei

| $E_d$ MeV | Potential set | V MeV | $r_v$ fm | $a_v$ fm | $N_r$ | W MeV | $r_w$ fm | $a_w$ fm |
|---|---|---|---|---|---|---|---|---|
| 11.8 | OM | 72 | 1.17 | 0.845 | | 13.0 | 1.322 | 0.509 |
| | DF | | | | 0.80 | 17.0 | 1.211 | 0.519 |
| 13.6 | OM | 80.70 | 1.17 | 0.993 | | 13.50 | 1.322 | 0.459 |
| | DF | | | | 0.80 | 15.5 | 1.225 | 0.459 |
| 14.5 | OM | 86.8 | 1.17 | 0.993 | | 17.50 | 1.322 | 0.505 |
| | DF | | | | 0.80 | 15.5 | 1.250 | 0.455 |
| 27.7 | OM | 83.13 | 1.17 | 0.845 | | 16.251 | 1.322 | 0.512 |

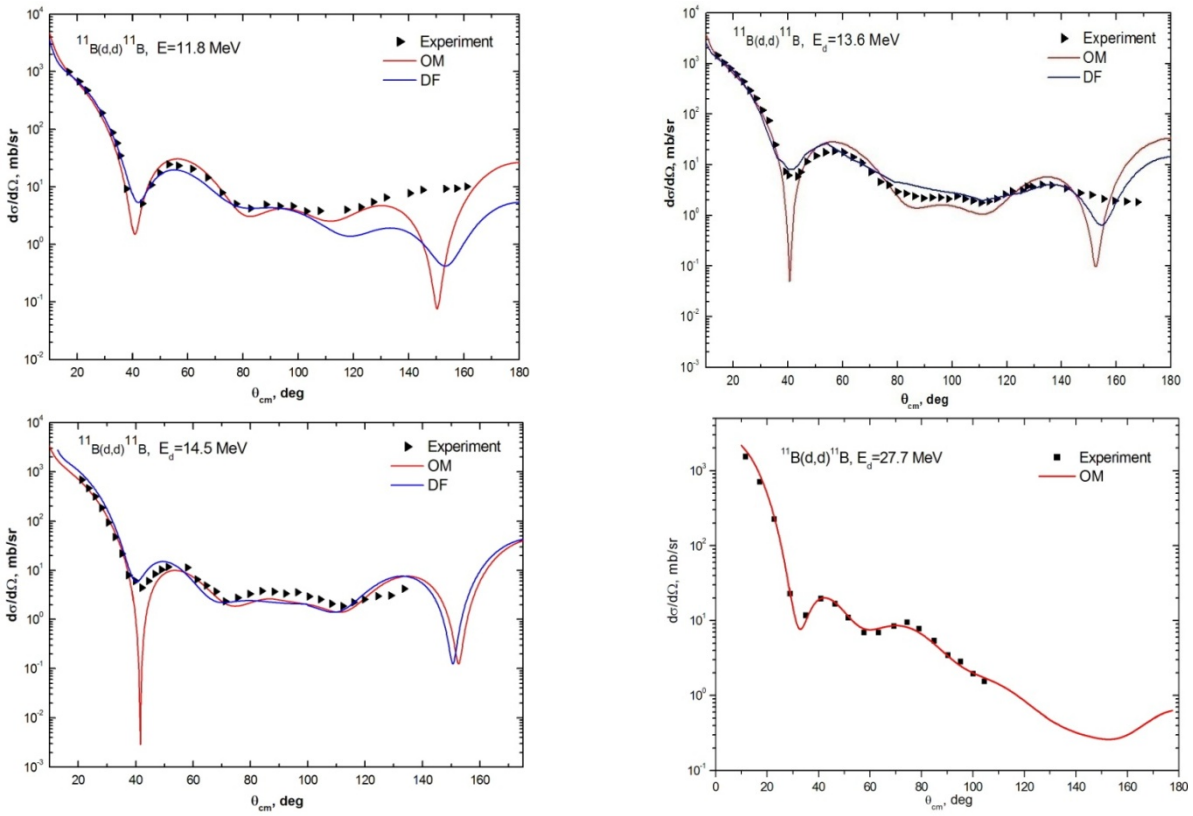


Symbols – experimental data for elastic scattering; solid curves – calculations within OM and DF.

**Figure 2** – Angular distributions of elastic scattering of deuterons from $^{11}$B nuclei at energies 11.8, 13.6 and 14.5 MeV in comparison with calculated differential cross sections

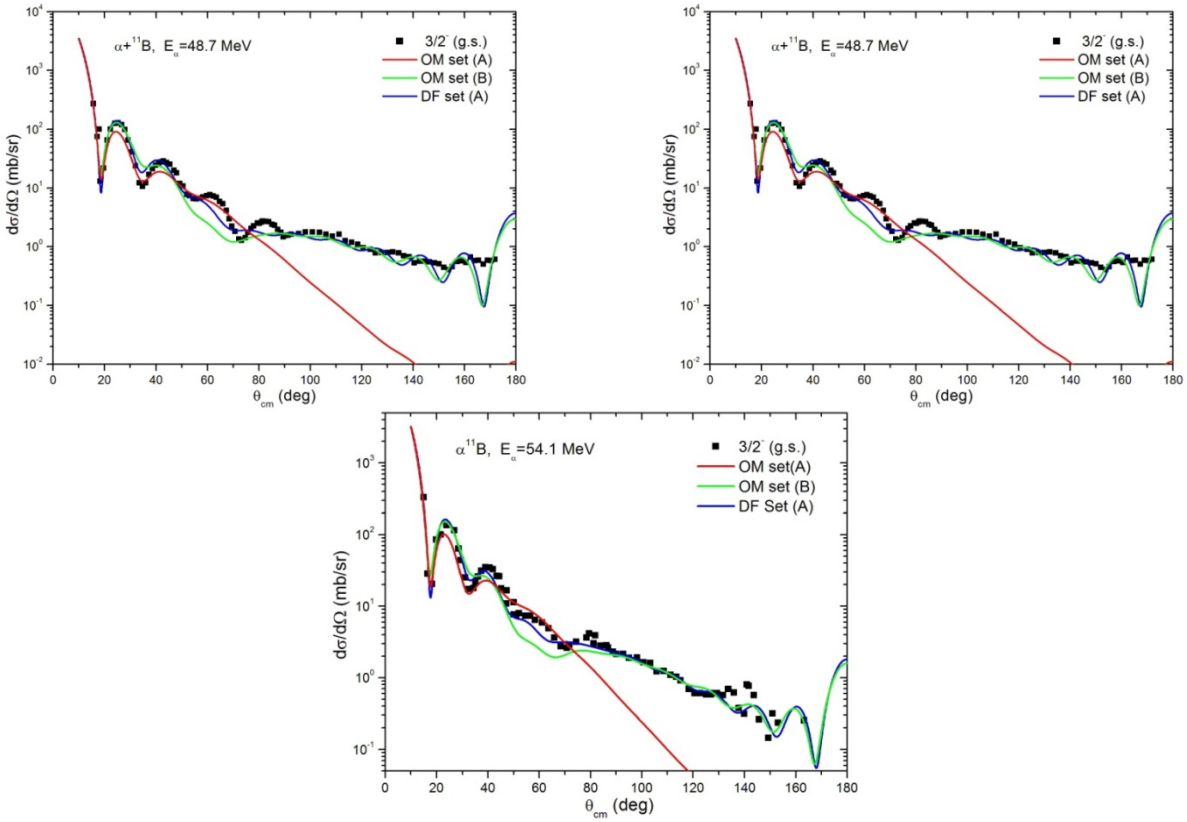


Symbols – experimental data for elastic scattering; solid curves – calculations within OM and DF.

**Figure 3** – Angular distributions of elastic scattering of alpha particles from $^{11}$B nuclei at energies 48.7, 50.5 and 54.1 MeV in comparison with calculated differential cross sections

**Table 2** – Parameters of optical and folding potentials for deuterons scattering from $^{11}$B nuclei

| E MeV | Potential set | $V_o$ MeV | $r_v$ fm | $a_v$ fm | Nr | W MeV | $r_w$ fm | $a_w$ fm | $J_V$ MeV fm$^3$ | Jw MeV fm$^3$ |
|---|---|---|---|---|---|---|---|---|---|---|
| 48.7 | OM A | 76.0 | 1.245 | 0.825 | | 15.89 | 1.57 | 0.801 | 200 | 95.4 |
| | OM B | 123.0 | 1.245 | 0.74 | | 18.91 | 1.57 | 0.623 | 388 | 106.7 |
| | DF A | | | | 1.3 | 23.32 | 1.57 | 0.547 | | 99.01 |
| 50.5 | OM A | 77.22 | 1.245 | 0.856 | | 16.85 | 1.57 | 0.833 | 260 | 102.4 |
| | OM B | 120.0 | 1.245 | 0.752 | | 18.14 | 1.57 | 0.731 | 381 | 106.1 |
| | DF A | | | | 1.2 | 18.14 | 1.57 | 0.731 | | |
| | DF B | | | | 1.2 | 30.0 | 1.33 | 0.746 | | 112.9 |
| 54.1 | OM A | 80.73 | 1.245 | 0.822 | | 15.08 | 1.57 | 0.85 | 266 | 92.2 |
| | OM B | 125.0 | 1.245 | 0.746 | | 19.56 | 1.57 | 0.628 | 396 | 110.6 |
| | DF A | | | | 1.28 | 23.5 | 1.57 | 0.552 | | 113.3 |

**Inelastic scattering**

The comparison between the experimental data and theoretical predictions for the $1/2^-$ (2.125 MeV), $5/2^-$ (4.445 MeV), $7/2^-$ (6.743 MeV) and "exotic" $3/2^-$ (8.56 MeV) states at $E_d$=14.5MeV and $E_\alpha$=29, 40.5 [4], 50.5[4], 65 [15] MeV are shown in figures 4,5 and 6 respectively. The theoretical calculations of the angular distributions for the different excited states were performed using the coupled channel method implemented in code Fresco using different potential sets. The extracted deformation parameters for the $1/2^-$ (2.125 MeV), $5/2^-$ (4.445 MeV), $7/2^-$ (6.743 MeV) and "exotic" $3/2^-$ (8.56 MeV) states at energies 29, 40 and 50 MeV are listed in table 3

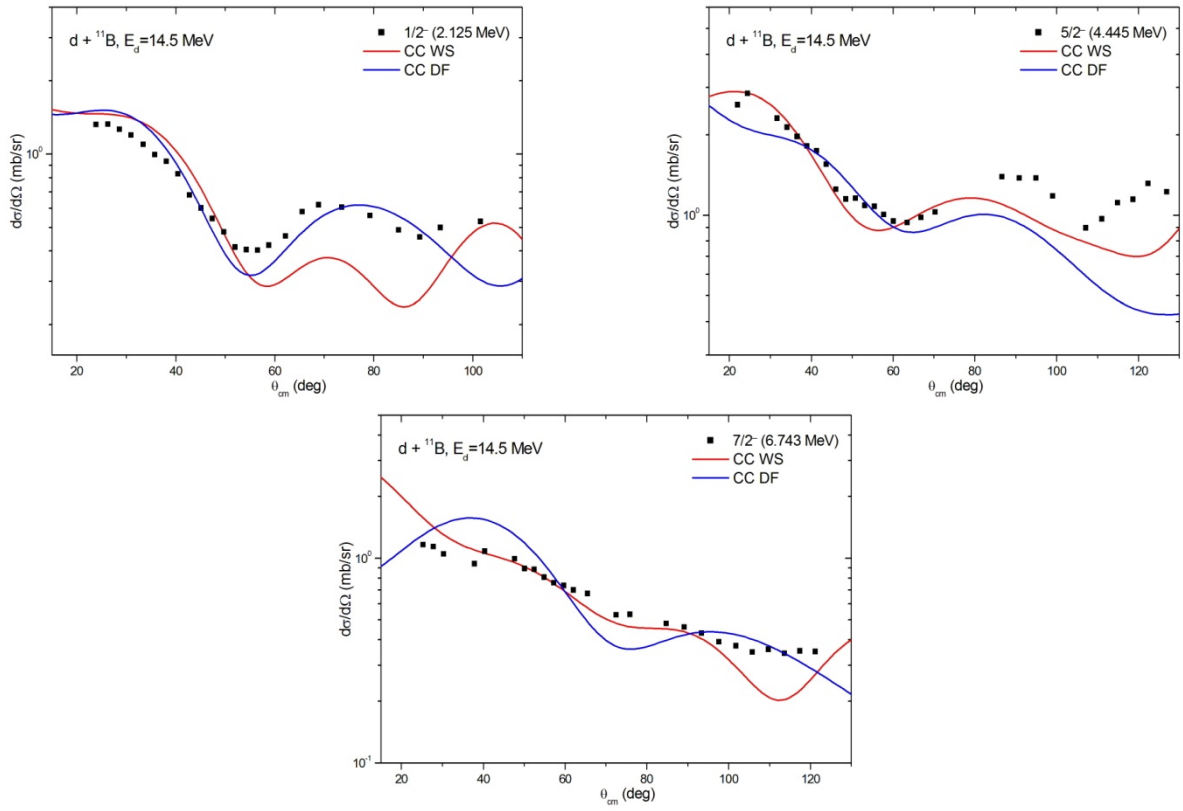


Symbols – experimental data for elastic scattering; solid curves – calculations within CC.

**Figure 4** – Angular distributions of inelastic scattering of deuterons from $^{11}$B nuclei at $E_d$=14.5 MeV in comparison with calculated differential cross sections

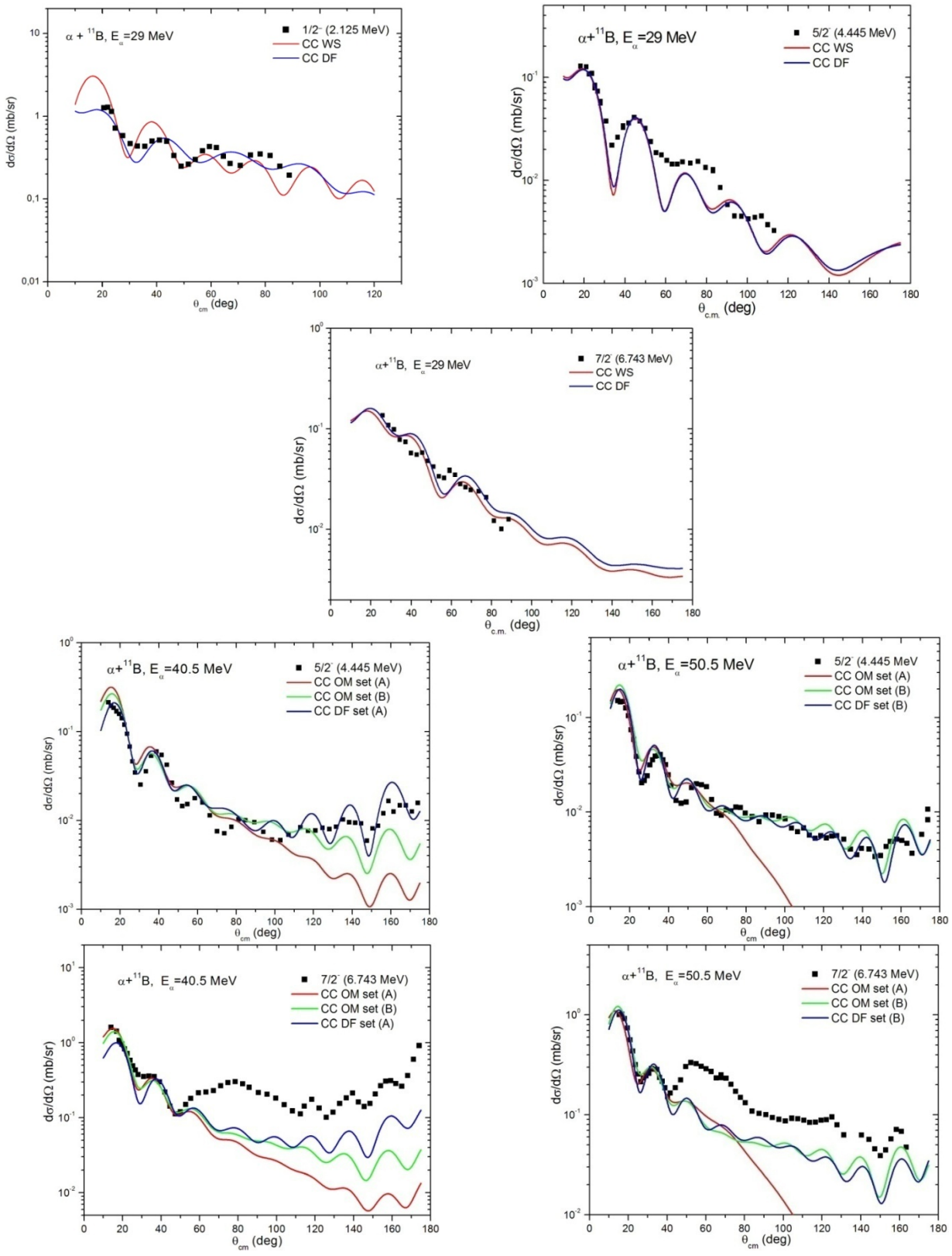


Symbols – experimental data for elastic scattering; solid curves – calculations within CC.

**Figure 5** – Angular distributions of inelastic scattering of alpha particles from $^{11}$B nuclei at $E_\alpha$=29, 40.5 and 50.5 MeV in comparison with calculated differential cross sections

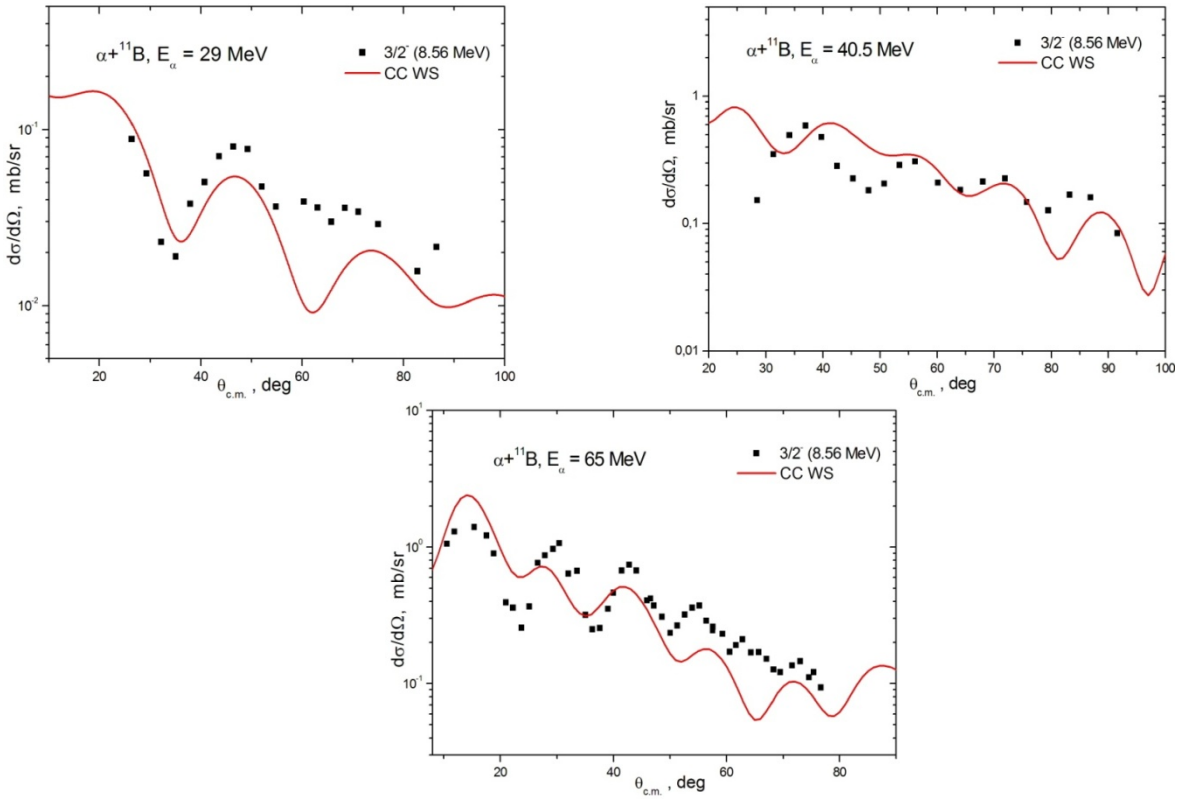


Symbols – experimental data for elastic scattering; solid curves – calculations within CC.

**Figure 6** – Angular distributions of inelastic scattering of alpha particles from $^{11}$B nuclei at $E_\alpha$=29, 40.5, 65 MeV in comparison with calculated differential cross sections

**Table 3** – Deformation parameters of $^{11}$B excited states

| $E_{lab}$, MeV | Potential | β (1/2$^-$) | β (5/2$^-$) | β (7/2$^-$) | β (3/2$^-$) |
|---|---|---|---|---|---|
| 14.5 ($E_d$) | WS | 0.46 | 0.47 | 0.47 | |
| | DF | 0.47 | 0.45 | 0.47 | |
| 29 ($E_\alpha$) | WS | 0.45 | 0.46 | 0.44 | 0.41 |
| | DF | 0.45 | 0.46 | 0.44 | |
| 40.5 ($E_\alpha$) | WS | | 0.42 | 0.42 | 0.42 |
| | DF | | 0.4 | 0.42 | |
| 50.5 ($E_\alpha$) | WS | | 0.35 | 0.4 | |
| | DF | | 0.35 | 0.4 | |
| 65 ($E_\alpha$) | WS | | | | 0.42 |

## Nuclear radii

The root mean square (rms) radii of 3/2$^-$ (0 MeV), 1/2$^-$ (2.125 MeV), 5/2$^-$ (4.445 MeV), 7/2$^-$ (6.743 MeV) and "exotic" 3/2$^-$ (8.56 MeV) states were estimated within the modified diffraction model (MDM) [16]. This method allows determining rms radius $\langle R^* \rangle$ of the excited state via the difference of diffraction radii of the exited and the ground states using the expression

$$R^* = R_0 + \left[R^*_{dif} - R_{dif}(0)\right] \quad (4)$$

Here $R_0$ is the rms of the ground state of the studied nucleus, $R^*_{dif}$ and $R_{dif}(0)$ are the diffraction radii determined from the positions of the minima and maxima of the experimental angular distributions of elastic and inelastic scattering correspondingly. The rms radii of $3/2^-$ (0 MeV), $1/2^-$ (2.125 MeV), $5/2^-$ (4.445 MeV), $7/2^-$ (6.743 MeV) states are given in table 4 at $E_\alpha$=29, 40.5 [5], 50.5 [5] and 65 [15] MeV. The radius of "exotic" $3/2^-$ (8.56 MeV) state was determined at $E_\alpha$=29, 40.5 MeV. The obtained radii are in fair agreement with the results obtained in other works within MDM[16] and other approaches for determining the radii of excited states, such as antisymmetrized molecular dynamics (AMD) [17] and orthogonality condition model (OCM). The comparison of

**Table 4** – Root mean square radii of ground and excited states of $^{11}$B, obtained within MDM

| $E_{lab}$, MeV | $R_{rms}$ (0.00), fm | $R_{rms}$ (2.12), fm | $R_{rms}$ (4.445), fm | $R_{rms}$ (5.02), fm | $R_{rms}$ (6.74), fm |
|---|---|---|---|---|---|
| 29 | 2.29 | 2.33±0.10 | 2.25 ±0.12 | | 2.25 ± 0.15 |
| 40.5 [4] | 2.29 | | 2.17±0.08 | | 2.22 ± 0.10 |
| 50.5 [4] | 2.29 | | 2.30±0.15 | | 2.31 ± 0.11 |
| 65 [15] | | 2.37 ±0.20 | 2.27±0.10 | 2.44±0.14 | 2.32 ± 0.14 |

**Table 5** - Root mean square radius of $3/2^-$ (8.56 MeV) state

| | MDM ($E_\alpha$=29 MeV) | MDM ($E_\alpha$=40.5 MeV) | MDM [16] ($E_\alpha$=65 MeV) | AMD [17] | OCM [18] |
|---|---|---|---|---|---|
| $R_{rms}$ (fm) | 2.88 ± 0.16 | 2.84 ± 0.12 | 2.87 ± 0.13 | 3.1 | 3.0 |

## Results and Conclusion

The experimental angular distributions of elastic and inelastic scattering of deuterons from $^{11}$B nuclei have pronounced diffraction pattern in the whole angular range. There is a notable enhancement at backward angles, this can be due to the contribution of other mechanisms to the scattering cross sections (contribution of compound nucleus, resonance scattering etc.). The calculated differential cross sections are in fairly good agreement with the experimental data.

The estimated radii of $3/2^-$ (8.56 MeV) state is increased with respect to the radius of ground states and are good agreement with literature data that were obtained using different approaches indicating that the radius of this state is indeed increased. Thus, the expected cluster structure of this state is verified.

## References

1. Bulter J.W. Table of (p,γ) resonances by proton energy: E = 0.163 – 3.0 MeV. // U.S. Naval Research Laboratory. NRL Report. – 1959. – P. 5282-5299.

2. W. Fitz, R. Jahr, R. Santo. Scattering and pick-up reactions with deuterons on Be, B,C,N and O at 11.8 MeV // Nuclear Physics. Section A. – 1967. – Vol. 101 .– P .449.

3. A.N. Vereshchagin, I.N. Korostova, L.S. Sokolov, V.V.Tokarevskii, I. P.Chernov. Investigation of elastic scattering of deuterons on light nuclei with 13.6 MeV energy // Bull. Russian Academy of Sciences. – Physics. – 1969. – Vol. 32. – P.573.

4. Slobodrian R.J. Scattering of 27.7 MeV deuterons on beryllium and boron // Nuclear Physics. – 1962. – Vol. 32. – P.684–694.

5. Burtebaev N., Baktybaev M.K., Duisebaev B.A., Peterson R. J., and Sakuta S. B. Scattering of

α Particles on 11B Nuclei at Energies 40 and 50 MeV // Physics of Atomic Nuclei. – 2005. – Vol. 68. – P. 1303–1313.

6. Abele H. et al. Measurement of Folding-Potential Analysis of the Elastic α-Scattering on Light Nuclei // Zeitschrift für Physik A Atomic Nuclei. – 1987. – Vol. 326. – P. 373–381.

7. Thompson I.J. Coupled reaction channels calculations in nuclear physics // Comput. Phys. Re. – 1988. – Vol. 7. – P. 167–212.

8. Bertsch G, Borysowicz J, Mc Manus H and Love W G. Interactions for inelastic scattering derived from realistic potentials // Nucl. Phys. A. – 1977. – Vol. 284. – P. 399-419.

9. Anantaraman N, Toki H and Bertsch G An effective interaction for inelastic scattering derived from the Paris potential // Nucl. Phys. A. – 1983. – Vol. 398. – P. 269-278.

10. Satchler G.R. and Love W.G. Folding model potentials from realistic interactions for heavy-ion scattering // Phys. Re. – 1979. – Vol. 55. – P. 183-254.

11. Jeukenne J, Lejeune A and Mahaux C Optical-model potential in finite nuclei from Reid's hard core interaction // Phys. Rev. C. – 1977. – Vol. 16. – P. 80.

12. Kobos A.M., Brown B.A., Hodgson – P.E., Satchler G.R. and Budzanowski A. Folding model analysis of α-particle elastic scattering with a semirealistic density-dependent effective interaction // Nucl. Phys. A. – 1982. – Vol. 384. – P. 65-87.

13. Kobos A.M., Brown B.A., Lindsay R. and Satchler G.R. Folding-model analysis of elastic and inelastic α-particle scattering using a density-dependent force // Nucl. Phys. A. – 1984. – Vol. 425. – P. 205-232

14. Brandan M.E. and Satchler G.R. Folding model analysis of 12,13C+12C and 16O+12C scattering at intermediate energies using a density-dependent interaction // Nucl. Phys. A. – 1988. – Vol. 487.– P. 477-492

15. Danilov A. N. et al. Study of Elastic and Inelastic 11B +α Scattering and Search for Cluster States of Enlarged Radius in 11B // Physics of Atomic Nuclei. – 2015. – Vol. 78. – P. 777–793.

16. Danilov A.N., Belyaeva T.L., Demyanova A.S., Goncharov S.A. and Ogloblin A.A. Determination of nuclear radii for unstable states in 12C with diffraction inelastic scattering // Physical Review C. – 2009. – Vol. 80. – P. 054603

17. Suhara T. and Kanada-En'yo Y. Cluster structures in 11B // Phys. Rev. C. – 2012. – Vol. 85.– P. 054320

18. Yamada T. and Funaki Y. α + α + t cluster structures and 12C($0_2^+$)-analog states in 11B // Phys. Rev. C. – 2010. – Vol.82. – P. 064315